JOURNAL OF MATERIALS PROCESSING TECHNOLOGY 209 (2009) 2321–2328

journal homepage: www.elsevier.com/locate/jmatprotec

Numerical simulation of the twin-roll casting process of magnesium alloy strip

Jian Zeng[a,*], *Roger Koitzsch*[b], *Herbert Pfeifer*[b], *Bernd Friedrich*[a]

[a] *IME Institute for Process Metallurgy and Metal Recycling, RWTH Aachen University, Intzestrasse 3, 52056 Aachen, Germany*
[b] *Institute for Industrial Furnaces and Heat Engineering, RWTH Aachen University Kopernikusstraße 16, 52074 Aachen, Germany*

ARTICLE INFO

Article history:
Received 21 June 2007
Received in revised form
14 May 2008
Accepted 15 May 2008

Keywords:
Magnesium alloy strip casting
Melt-flow
Solidification
CFD-simulation

ABSTRACT

The magnesium twin-roll strip casting process is investigated with a test caster at the IME. The flow field in the melt cannot be investigated optically, therefore numerical simulations have been undertaken to show the flow field in the Mg melt, the solidification between the two rolls and the cooling of the strip. The three-dimensional, turbulent flow field for different steady state casting points, in the process gap, have been calculated, including the solidification of the magnesium alloy melt. Within the process gap of the casting process the flow field shows similar flow structures. A big vortex in the casting channel and a much smaller vortex between the two rolls occur. With the increase of the casting speed the mushy zone is moved towards the kissing point. This can be interpreted due to a smaller force on the rolls. Nevertheless, the solidification on the rolls is so strong, that rolling between the two rolls happens.

1. Introduction

The demand to reduce energy consumption increased the use of light-weight alloys in the automobile industry. As the lightest structural metal with a high specific strength and Young-module, magnesium and its alloys have been widely applied in this industrial area. Specially, strip products made from Mg wrought-alloys have been focused on because of their well-balanced mechanical properties. Liang and Cowley (2004) described the challenges faced in producing of magnesium alloy strip by twin roll casting as well as pilot plant test results. Engl (2005) reported that magnesium strips with a thickness of 4.5–7 mm were produced at competitive prices with the aid of twin-roll technology in Thyssenkrupp steel AG (Germany). Loechte et al. (2005) investigated the microstructures and mechanical properties of magnesium alloy sheet by twin roll casting. Their research is of particular relevance because the process parameters such as casting speed have been discussed.

The twin-roll thin strip casting process has been developed to produce magnesium alloy strip directly from its molten metal. Fig. 1 shows the basic principle of Mg twin-roll process: through a half-opening casting tip the magnesium-melt is transported to the casting gap (kissing point). The two counter-rotating rolls, which are water cooled from inside, together with the side-sealing dam, build a moving mould. As a result of the heat flux from the melt to the rolls, Mg melt solidifies and shapes into a strip and then is transported toward the kissing point.

This process combines casting and hot rolling into a single process, which introduces a solution to produce magnesium strip products at competitive costs for commercial applications. On the other hand, the thermo-physical properties of Mg alloys, for instance, the small volume-specific heat capacity and large 'mushy zone' (interval between liquidus and solidus

* *Corresponding author*. Tel.: +49 6181 35 9712; fax: +49 6181 35 3091.
E-mail address: jzeng@web.de (J. Zeng).
0924-0136/$ – see front matter © 2008 Elsevier B.V. All rights reserved.
doi:10.1016/j.jmatprotec.2008.05.032

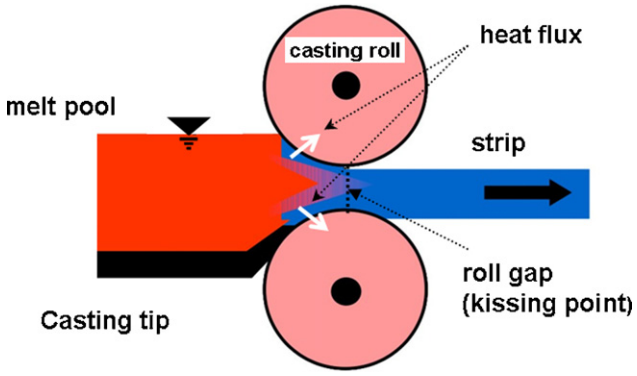

Fig. 1 – Principle of the twin-roll thin strip casting process according to the test caster in the IME.

temperature), make it difficult to develop the Mg twin-roll process. The investigation of complex melt flow and solidification phenomenon occurring during the casting process is essential to avoid surface and internal defects and improve the quality of casting strips. Furthermore, the influences of casting parameters, such as casting speed and casting gap, on the melt flow and solidification must also be considered, in order to build an optimized process-window. Experimental observations and CFD (computational fluid dynamics) simulations were both carried out at IME (Institute for process metallurgy and metal recycling) and IOB (Institute for industrial furnaces and heat engineering) institutes, respectively.

Different numerical models are presented by various authors. Hwang et al. (1996) suggested a constant heat transfer coefficient could be used in his CFD model to describe the thermal conduction between metal and rolls. Tavares and Guthrie (1998) concentrated their CFD-simulation on different metal delivery systems for twin roll casting. Buechner (2004) proposed a model to investigate the correlations between feeding system and strip quality. Ohler (2005) has done comprehensive CFD simulations of the process. In his research, the simulations of free surface wave have been carried out using a Volume of Fluid (VoF) model. Despite the general fundamental studies of numerical models, few focused on the Magnesium twin-roll process. Bae et al. (2007) examined the velocity and temperature distributions during the vertical twin- roll casting of Mg by a 2D FDM & FEM simulation. Ju et al. (2005) studied the effect of type and dimension of delivery nozzles on Mg twin-roll casting process by thermal flow FEM-simulation.

The CFD model presented in this paper provides us with a better understanding of the melt's flow characteristics and thermal exchanges during the rapid solidification of the Mg twin-roll casting process. The influence of casting speed and the gauge (twin-roll gap opening) on the melt flow and solidification are also discussed.

2. Numerical model

The basis for numerical flow simulations are the conservation laws of mass, momentum and energy. These differential equations lead to the RANS-equations (Reynolds Averaged Navier Stokes) with seven unknowns (Eqs. (1)–(3)). The system of partial differential equations can be solved using additional equations, such as the equation of state for the melt behaviour. The melt is treated as a Newtonian fluid.

$$\frac{\partial}{\partial x_i}(\rho \bar{u}_i) = 0 \tag{1}$$

$$\rho \bar{u}_j \frac{\partial \bar{u}_i}{\partial x_j} = \rho g_i - \frac{\partial \bar{p}}{\partial x_i} + \frac{\partial}{\partial x_j}\left[\mu\left(\frac{\partial \bar{u}_i}{\partial x_j} + \frac{\partial \bar{u}_j}{\partial x_i} - \frac{2}{3}\delta_{ij}\frac{\partial \bar{u}_l}{\partial x_l}\right)\right] + \frac{\partial}{\partial x_j}(-\rho\overline{u_i' u_j'}) \tag{2}$$

$$\frac{\partial}{\partial t}(\rho \bar{e}) + \frac{\partial}{\partial x_i}[\bar{u}_i(\rho \bar{e} + \bar{p})] = \frac{\partial}{\partial x_i}\left[\lambda_{\text{eff}}\frac{\partial \bar{T}}{\partial x_i} - \sum_m h_{mi} J_{mi} + \bar{u}_j(\tau_{ij})_{\text{eff}}\right] + \sum_k k_{mi} J_{mi} + S_h \tag{3}$$

Launder and Spalding (1974) proposed the standard $k-\varepsilon$ turbulence model to simulate the turbulent behaviour of the melt flow. Shih et al. (1995) developed the realizable $k-\varepsilon$ turbulence model, which is one of the successful developments. This model is based on the Boussinesq approximation in which the Reynolds stress is a function of the mean gradients of velocity similar to the molecular stress. Two additional differential equations are used to calculate the turbulent kinetic energy k (Eq. (4)) and the dissipation rate ε (Eq. (5)).

$$\frac{\partial(\rho \bar{u}_j k)}{\partial x_j} = \underbrace{\frac{\partial}{\partial x_j}\left(\mu\frac{\partial k}{\partial x_j}\right)}_{\text{mol. diffusion}} - \underbrace{\frac{\partial}{\partial x_j}\left(\frac{\rho}{2}\overline{u_j' u_i' u_i'} + \overline{p' u_j'}\right)}_{\text{turb. diffusion}} - \underbrace{\rho\overline{u_i' u_j'}\frac{\partial \bar{u}_i}{\partial x_j}}_{\text{production}} - \underbrace{\mu\overline{\frac{\partial u_i'}{\partial x_k}\frac{\partial u_i'}{\partial x_k}}}_{\text{dissipation}} \tag{4}$$

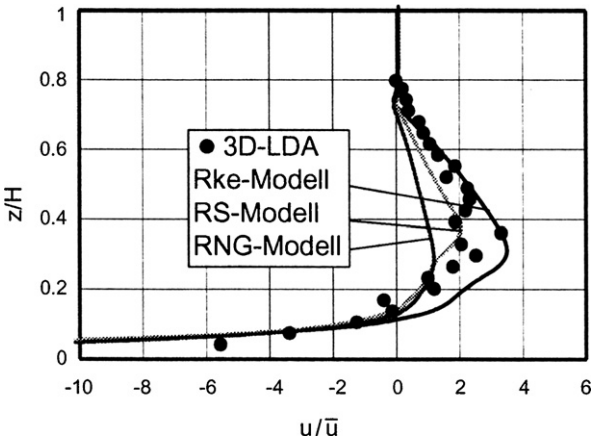

Fig. 2 – Comparison of the laser-based experimental measurements (3D-LDA) and the calculated values in a velocity profile. (Rke-Modell: realizable $k-\varepsilon$ model; RS-Modell: Reynolds stress model; RNG-Modell: RNG-$k-\varepsilon$ model).

$$\frac{\partial(\rho\bar{u}_j\varepsilon)}{\partial x_j} = \underbrace{\rho C_1 S_{ij}\varepsilon}_{\text{production}} + \underbrace{\frac{\partial}{\partial x_i}\left[\left(\mu + \frac{\mu_t}{Pr_{t,\varepsilon}}\right)\frac{\partial\varepsilon}{\partial x_i}\right]}_{\text{diffusion}} - \underbrace{C_2\rho\frac{\varepsilon^2}{k+\sqrt{\nu\varepsilon}}}_{\text{dissipation}} \quad (5)$$

The model is slightly more time consuming than the standard $k-\varepsilon$ turbulence model, but shows performance improvements for complex turbulent flows. Boelling (2003) went a step further and used the laser-based experiments to verify the validity of this turbulent model. According to his research, simulation results are in good agreement with experimental observations (Fig. 2). In the present paper the realizable $k-\varepsilon$ turbulence model was applied.

In addition to the turbulent modelling of the melt flow a solidification model is needed in order to be evaluated to simulate the solidification process of the melt's flow on the twin-rolls. Therefore the solidification enthalpy ΔH_m during the solidification of the Mg melt has to be considered. Two different methods can be used in order to model the solidification enthalpy. The first is the enthalpy porosity scheme where the solidification enthalpy is a sink or source term in the energy equation. The second method models the solidification enthalpy with a temperature-dependent heat capacity. Both methods have the same energetic effect on the melt flow. In this model the temperature-dependent heat capacity is used to model the solidification enthalpy.

The temperature-dependent enthalpy (H) of a system is given by:

$$H = H_{ref} + \int_{T_{ref}}^{T} c\,dT \quad (6)$$

If there is a phase change during the solidification enthalpy's variation has to be added in Eq. (6).

The heat capacity $c(T)$ is added in FLUENT as a piece-vice-linear function in the calculated temperature interval.

In addition to the solidification enthalpy, the melt solidification process needs to be simulated and two methods can be used. The first method is a sink or source in the momentum equation and the second method is an increasing viscosity within the solidification temperature interval. The real rheological behaviour of Mg melt is mostly unknown and the proposed methods are approximations to the real behaviour. The method used here models a sink in the momentum equation. Darcy's (1856) investigation on a water flow through sand is the basis of this method. Eq. (7) is applicable to Stokes flow and defines the notion of permeability. Using this relationship within the momentum equation means that the solidifying

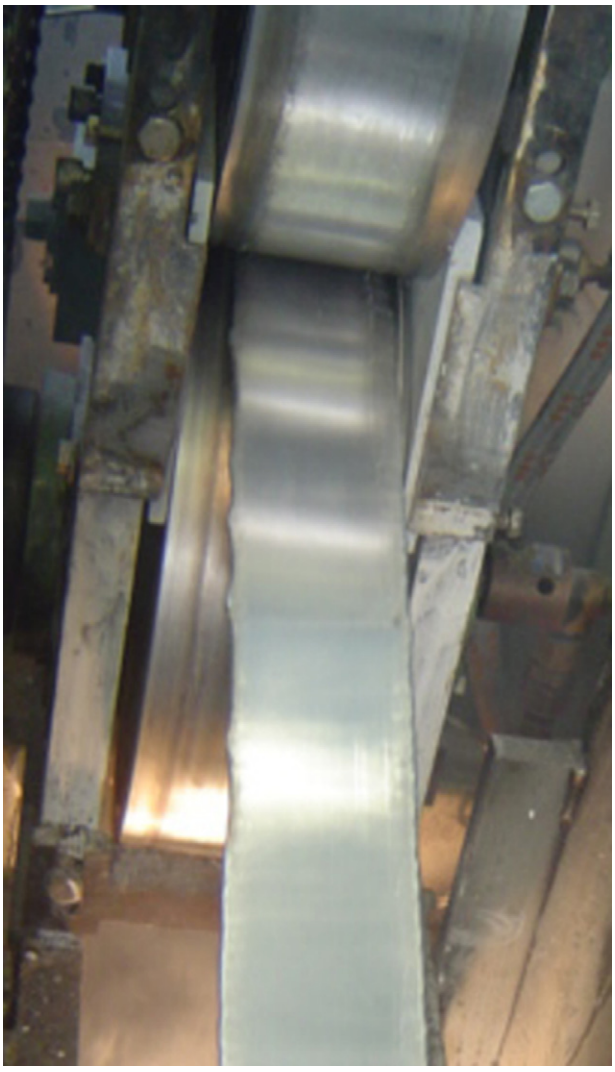

Fig. 3 – Twin-roll strip test caster at the IME and its geometrical setup: caster and cast strip.

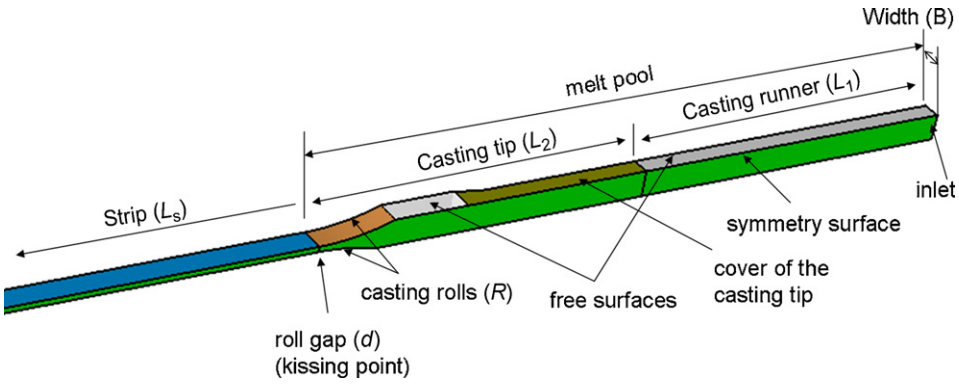

Fig. 4 – Twin-roll strip test caster at the IME geometrical setup: L_1 = 250 mm, L_2 = 225 mm, L_s = 1000 mm, B = 5 mm, R = 340 mm, d = 3 or 4 mm.

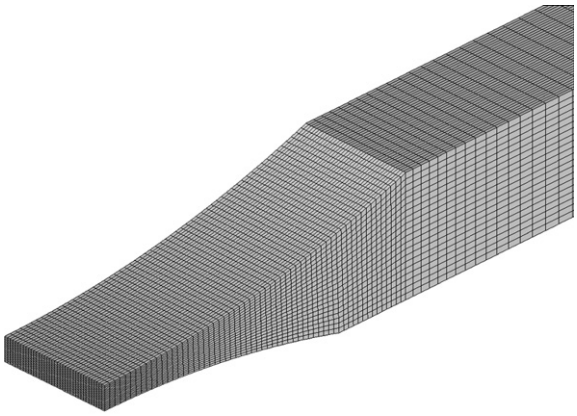

Fig. 5 – Numerical grid of the melt pool (detail) with a total number of grid cells about 130,000.

melt is considered as a porous media formed by the solidification microstructure, where the permeability of the mushy zone defines implicitly the varying viscosity of the solidifying melt.

$$\frac{d(\rho\bar{u}_i\bar{u}_j)}{dx_i} = \ldots - C\frac{(1-\beta)^2}{\beta^3+\varepsilon}(u_i - u_{P,i}) \quad (7)$$

where C is a constant of the liquid phase value between 104 and 107, β is the liquid phase

$$\beta = \frac{T - T_{sol}}{T_{liq} - T_{sol}} \quad (8)$$

$U_{P,i}$ is the one-dimensional pull velocity, ε is a small number to avoid division by zero. For the temperature $T = T_{liq}$ ($\beta = 1$) the additional term in Eq. (3) diminishes to zero. For $T = T_{sol}$ ($\beta = 0$) the velocity $U_{P,i}$ rises to the pull velocity. The melt and the solidified melt are treated as Newtonian fluids. The viscosity rises from $\mu = 10^{-3}$ Pa s up to $\mu = 10^4$ Pa s in the solidification interval $T_{sol} = 575\,^\circ\text{C} < T < T_{liq} = 630\,^\circ\text{C}$. The viscosity $\mu(T)$ follows the behaviour of the sink term in Eq. (2) to get a similar physical behaviour.

3. Geometrical setup and boundary conditions

The twin-roll strip caster at the IME (Fig. 3) has two rolls with a diameter of 340 mm and a width of 100 mm. The outer roll units made of steel are used for Mg strip casting instead of copper ones, in order to avoid extremely rapid solidification. The casting gauge varies from 2 to 5 mm and the casting speed from 0.26 to 5.11 m/min. A 3D geometry is built up for the simulations. The geometrical setups are given out according to the test caster at the IME (Fig. 4).

The block-structured grid is with 130,000 cells generated for the melt pool and 200,000 cells for the 1 m long strip. Considering the rotation and solidification of the melt on the casting rolls, the zone, where the melt is in contact with the casting rolls, is locally refined and defined as "moving wall" boundary condition (Fig. 5). A symmetry boundary condition surface is used so that only half of the melt flow is considered as the simulation domain.

Table 1 – Variation of roll gap (d) and casting speed v in the simulations

	v_1 (m/min)	v_2 (m/min)	v_3 (m/min)
$d = 3$ mm	3.6	3.8	4
$d = 4$ mm	2.5	3	3.3

Table 2 – Boundary conditions in the simulation

Boundary condition	Symbol	Value
Turbulence at the inlet	Tu in %	2
Diameter at the inlet	D in m	0.012
Casting temperature	T in °C	700
Melt pool/casting rolls, $T_{ref} = 100\,^\circ$C, $d = 4$ mm	α_1 in W/(m^{2}K)	3300
Melt pool/casting rolls, $T_{ref} = 100\,^\circ$C, $d = 3$ mm	α_1 in W/(m^{2}K)	4000
Melt pool/side sealing dams, $T_{ref} = 27\,^\circ$C	α_2 in W/(m^{2}K)	200
Melt pool/air, $T_{ref} = 27\,^\circ$C	λ in W/(mK)	20
Strip/air, $T_{ref} = 27\,^\circ$C[a]	α_3 in W/(m^{2}K)	12

[a] Here the heat transfer coefficient is used and appropriate to the emission's coefficient of heat radiations from strip to air.

A typical magnesium wrought alloy, MgAZ31 (3% Al, 1% Zn), is used. Its thermo physical properties, including density, specific heat, latent heat, thermal conductivity and viscosity, are used in the simulations.

The flow in the melt pool is dominated by interactions between the process parameters such as casting speed and gauge. To assess the influence of these process parameters on the melt flow and the solidification, a few parameter groups are investigated, all listed in Table 1. Different simulation results for varying casting speeds and gauges are in good agreement with experimental observations. Zeng (2007) has discussed comprehensive comparisons between the numerical and experimental results in detail and the conclusion here has been confirmed. Table 2 shows the boundary conditions, which are used in the simulation.

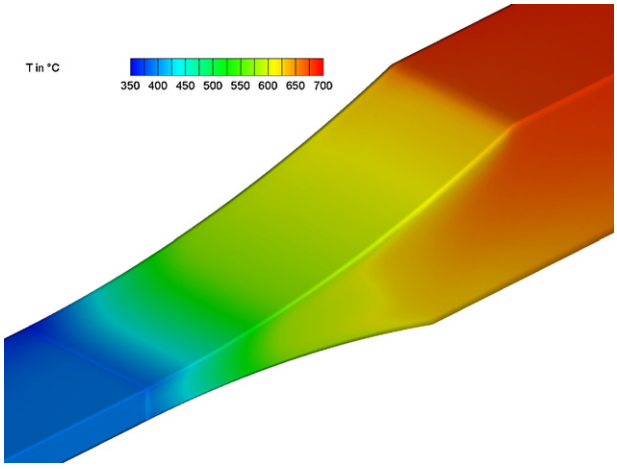

Fig. 6 – Temperature field of Mg surface in the regime of the rolls ($d = 4$ mm, $v = 2.5$ m/min).

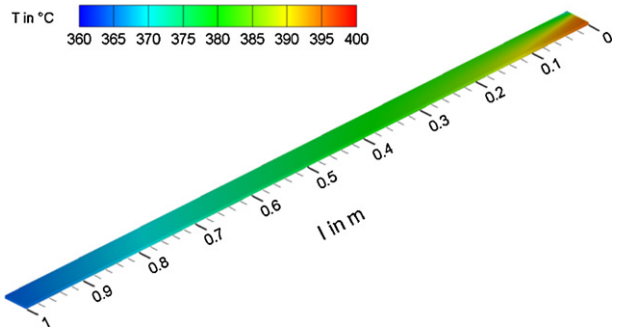

Fig. 7 – Temperature field of the cast strip ($d = 4$ mm, $v = 2.5$ m/min).

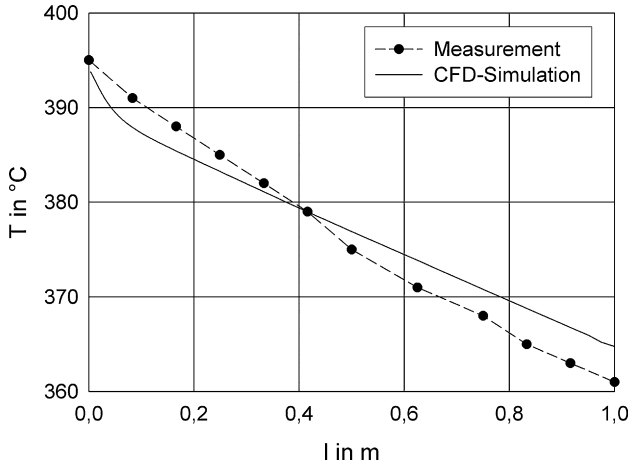

Fig. 8 – Temperature profiles of the cast strip ($d = 4$ mm, $v = 2.5$ m/min).

4. Results

To discuss general temperature and melt flow fields, the simulation at $d = 4$ mm, $v = 2.5$ m/min is taken as a typical case.

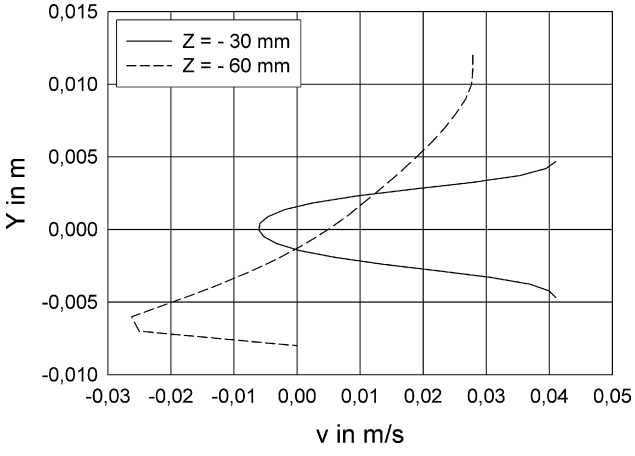

Fig. 9 – Velocity profile of the melt flow at $Z = -60$ mm and $Z = -30$ mm ($d = 4$ mm, $v = 2.5$ m/min).

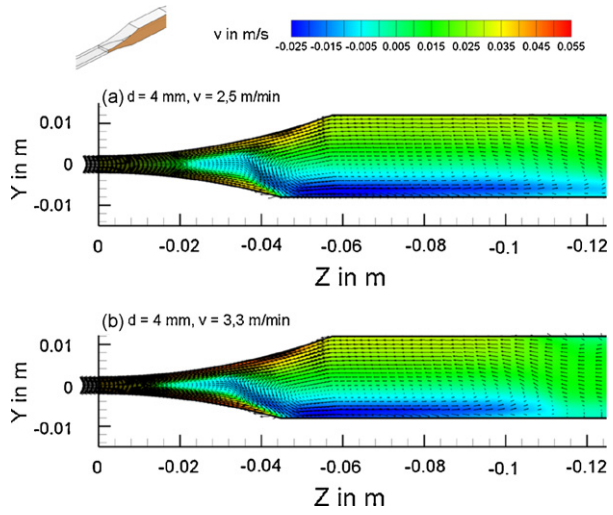

Fig. 10 – Flow field in the region of the casting rolls with a roll gap of $d = 4$ mm, (a) $v = 2.5$ m/min, (b) $v = 3.3$ m/min.

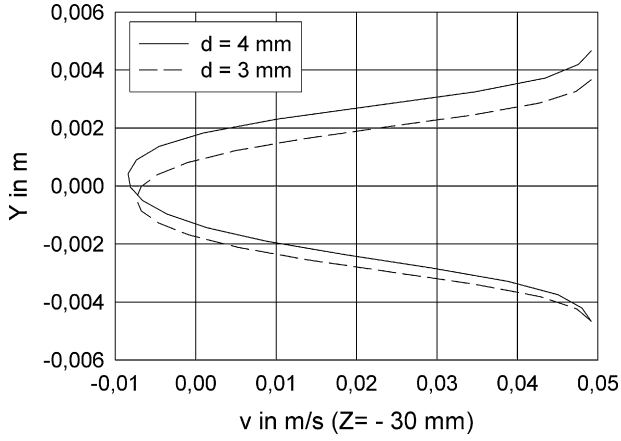

Fig. 11 – Velocity profiles of the melt flow with $d = 4$ mm and $d = 3$ mm at $Z = -30$ mm.

4.1. *Temperature field*

Fig. 6 shows the rapid solidification that the temperature decreases abruptly from 700 °C before the contact zone with casting rolls to about 390 °C at the kissing point. Considering the solidus temperature 575 °C, it suggests that the solidification of the Mg alloy is fully complete before leaving the kissing point and a strong rolling effect is expected. Ohler (2005) and Shih et al. (1995) determined that steel solidifies just at the kissing point during the process of twin-roll casting, which introduces a relative small rolling force (0.3–0.5 kN/mm). Zeng and Friedrich (2007) investigated the correlation between the rolling force and process parameters experimentally. The results demonstrate, comparing with steels, a much higher rolling force (4–10 kN/mm) was acquired during Mg twin-roll casting at the IME test caster.

After leaving the kissing point, the temperature of the 1 m long strip decreases slowly from 400 to 360 °C by means of heat emission into the air, Fig. 7. The cooling rate was approx. 1.67 °C/s. Simulation results are in good agreement with measured data as shown in Fig. 8.

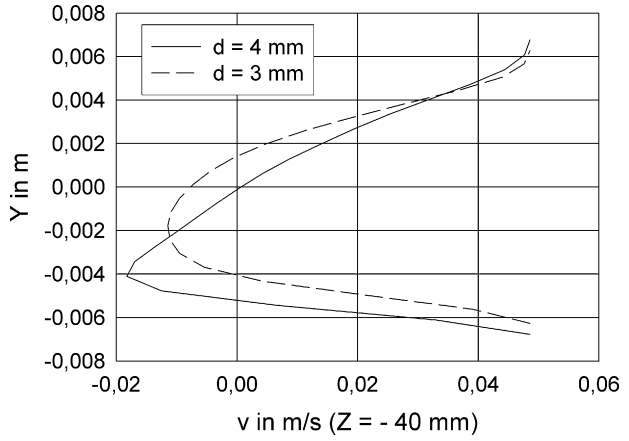

Fig. 12 – Velocity profiles of the melt flow with $d = 4$ mm and $d = 3$ mm at $Z = -40$ mm.

4.2. *Flow field*

Fig. 9 shows the velocity profiles in two zones in the melt pool. One at $Z = -60$ mm, where the melt flow has the first contact with the upper roll and the solidification begins. The second one at $Z = -30$ mm, where the alloy is in the 'mushy zone'. At $Z = -60$ mm a maximum reversed flow of -0.026 m/s near the bottom of the cast tip ($Y = -6$ mm) is calculated. The reverse flow is caused by the friction between the melt and the cast tip as well as the braking effect due to the lower roll. Then the melt is accelerated by the rolls and flows with a relatively high velocity into the gap. At $Z = -30$ mm, the reversed flow is very small ($v = -0.006$ m/s) and is symmetrically placed between the casting roles ($Y = 0$ mm).

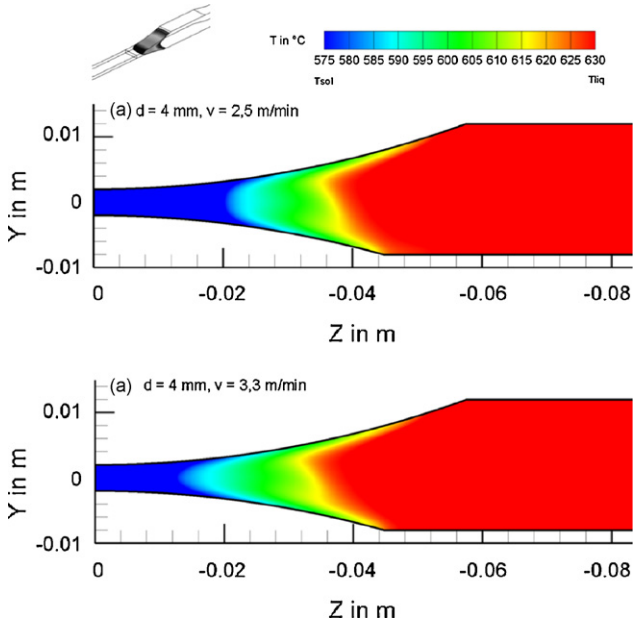

Fig. 13 – Solidification interval ('mushy zone') of the melt with $d = 4$ mm (a) at $v = 2.5$ m/min and (b) $v = 3.3$ m/min. (For interpretation of the references to color in this citation of figure, the reader is referred to the web version of the article.)

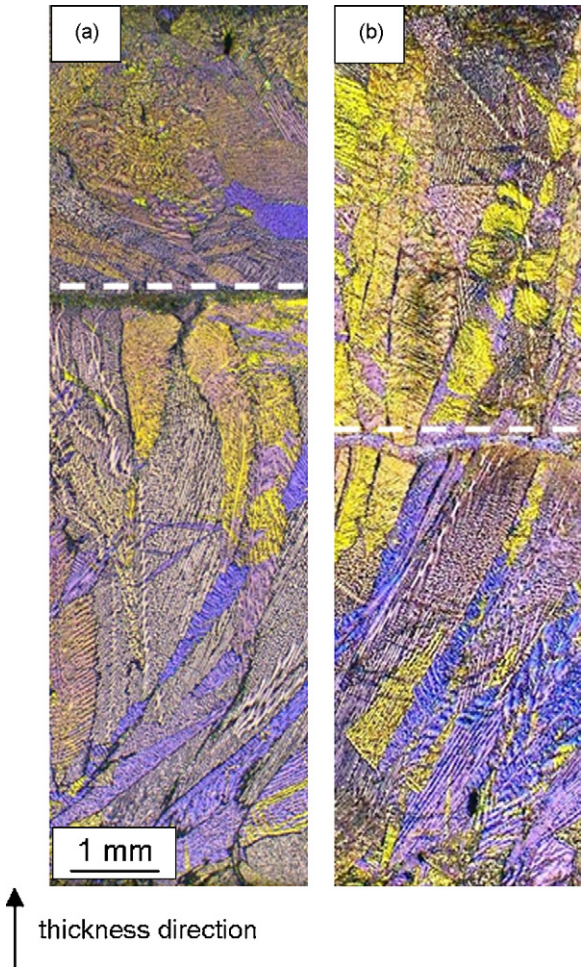

Fig. 14 – Microstructures of Mg strip, (a) with an asymmetrical flow; (b) with a symmetrical flow.

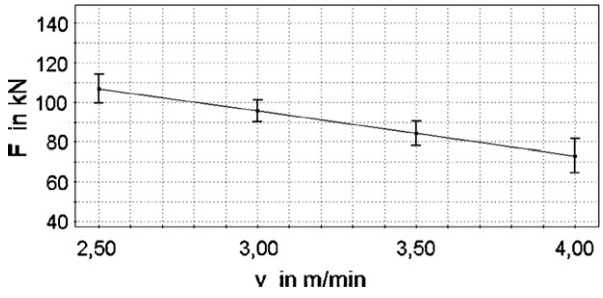

Fig. 15 – Effects of different velocities on the rolling force with a roll gap of $d = 4$ mm.

4.3. *Influence of parameters on the flow field*

Fig. 10 shows the flow field with variable speeds at a roll gap of $d = 4$ mm. The flow profiles at different roll speeds are similar, even though the absolute values of flow velocities differ. The flow field shows a reversed flow at the bottom of the casting channel, which forms a vortex. The reverse flow occurs near the bottom of the cast gate and in the middle zone between two rolls, which has been also shown in Fig. 10.

By comparing Fig. 10a with b, it can be concluded that, with a higher casting speed, the reverse flow decreases. A smaller vortex is formed between the casting rolls, with an additional reversed flow.

The influence of the rolling gap on the velocity is shown in Figs. 11 and 12. The velocity profiles in the mushy zone ($Z = -30$ mm) and just before solidification zone ($Z = -40$ mm) are discussed. At $Z = -30$ mm (Fig. 11), both velocity profiles have nearly axial symmetry and show a similar shape. Owing to the effects of flow on the solidification, the symmetrical flow conditions between the upper and lower rolls result in symmetrical dendrites, which were observed in experiments (Fig. 13). A strong asymmetrical upstream flow, with a higher reversed flow velocity, can be seen for the larger gap of $d = 4$ mm (Fig. 12). This result can be attributed to the deferent length of the contact zone between Mg melt and the upper or lower roll, which occurs because of the adjustment the gap by moving the upper roll. For this reason, a symmetrical movement of the rolls to form the gap and a similar length of the contact zone of both rolls should be ensured, in order to acquire a more symmetrical incoming flow (Fig. 14).

4.4. *Influence of the parameters on solidification interval*

Friedrich and Mordike (2006) suggested, in contrast to steel, Mg alloys have a large solidification zone beginning at 630 °C and terminating at 575 °C during which surface or bulk defects can be formed. Fig. 13 shows an increasing mushy zone with a rising casting speed. Moreover, attention should be paid to the length of the solidified zone in the melt pool, on which the roll force F dependents. At the same casting gauge of $d = 4$ mm, the length of the solidified zone with $v = 2.5$ m/min is approx. 22 mm (Fig. 13a, blue zone), which is much longer than this with $v = 3.3$ m/min (Fig. 13b, blue zone, approx. 15 mm). As a result, the rolling force under the condition of $v = 2.5$ m/min is much larger than under the condition of $v = 3.3$ m/min in agreement with experimental measurements (Fig. 15).

5. Conclusion

A CFD model for the numerical simulation of Mg twin-roll casting process has been developed. The turbulence in the melt pool is calculated with the realizable $k-\varepsilon$ turbulence model. An increased thermal capacity in terms of the solidification enthalpy and a temperature-dependent viscosity for the influence of the solidification on the melt flow was used in order to take the formation of the mushy zone into account. All the geometrical setup is built up according to the experiments. Series of simulations for different thermal and flow boundaries are carried out.

The calculated temperature field shows, that the temperature of melt pool decreases about 310 °C during the twin-roll process, which suggest that the melt solidifies completely before leaving the kissing point. Furthermore, the temperature distribution in a 1 m long strip is also simulated. The good agreement between the simulated and the measured values confirms the validity of the model. Reversed flows are observed in the simulation.

This numerical study shows the influence of the casting speed and the gauge on the flow and solidification field. An increasing casting speed results in a smaller reverse flow. Different casting gauges change the velocity profiles and a more symmetrical profile ensures a symmetrical microstructure. An increasing casting speed results also in an increasing mushy zone just before the kissing point; reducing the rolling force necessary for the formation of the strip as confirmed by experimental measurements.

Acknowledgement

J. Zeng gratefully acknowledges the financial support of the Germen Academic Exchange Service (DAAD).

REFERENCES

Bae, J.W., Kang, C.G., Kang, S.B., 2007. Mathematical model for the twin roll type strip continuous casting of magnesium alloy considering thermal flow phenomena. Journal of Materials Processing Technology 191, 251–255.

Boelling, R., 2003. Numerische und physikalische Simulation der stationaeren und instationaeren Stroemung in Stranggiessverteilern, first ed. Grips Media, Bad Harzburg.

Buechner, A.R., 2004. Thin strip casting of steel with a twin-roll caster—correlations between feeding system and strip quality. Steel Research 75, 5–12.

Darcy, H., 1856. Determination of the laws of flow of water through sand. In: Freeze, R.A., Back, W. (Eds.), Physical Hydrogeology. Van Norstramd Reinhold, New York, pp. 14–19 (English translation by Freeze, R.A.).

Engl, B., 2005. A new technology for magnesium sheet production. Light metal age 63, 14–19.

Friedrich, H.E., Mordike, B.L., 2006. Magnesium Technology: Metallurgy, Design Data, Applications. Springer, Berlin.

Hwang, J.D., Lin, H.J., Jang, S.C., Hwang, W.S., Hu, C.T., 1996. Relationship between flow characteristics and surface quality in inclined twin roll casting. ISIJ International 36, 690–699.

Ju, D.Y., Zhao, H.Y., Hu, X.D., Ohori, H., Tougo, M., 2005. Thermal flow simulation on twin roll casting process for thin strip production of magnesium alloy. Materials Science Forum 488/489, 439–444.

Launder, B.E., Spalding, D.B., 1974. The numerical computation of turbulent flows. Computer Methods in Applied Mechanics and Engineering 3, 269–289.

Liang, D., Cowley, C.B., 2004. The twin-roll strip casting of magnesium. JOM 56, 26–28.

Loechte, L., Westengen, H., Rodseth, J., 2005. An efficient route to magnesium alloy sheet: twin roll casting and hot rolling. In: Neelameggham, N.R., Kaplan, H.I., Powell, B.R. (Eds.), Magnesium Technology 2005,. Publication of TMS (The Minerals, Metals & Materials Society), Warrendale, pp. 247–252.

Ohler, C., 2005. Physical and Numerical Simulation of Fluid Flow and Solidification at the Twin-roll Strip Casting Process, first ed. Grips Media, Bad Harzburg.

Shih, T.-H., Liou, W.W., Shabbir, A., Yang, Z., Zhu, J., 1995. A new $k-\varepsilon$ eddy viscosity model for high Reynolds-number turbulent flows. Computers Fluids 24, 227–238.

Tavares, R.P., Guthrie, R.I.L., 1998. Computational fluid dynamics applied to twin-roll casting. Canadian Metallurgical Quarterly 37, 241–250.
Zeng, J., 2007. Einfluss der Stroemung und Erstarrungsbedingungen auf die Homogenitaet kontinuierlich gegossener Magnesium Duennband, first ed. Shaker, Aachen, pp. 71–84.
Zeng, J., Friedrich, B., 2007. Auswirkungen der Prozessparameter auf Bandqualitaet bei Duennbandgiessen nach dem Zwei-Rollen-Verfahren. Metall 61, 554–559.